Amino Acids (2020) 52:313–326
https://doi.org/10.1007/s00726-019-02764-9

ORIGINAL ARTICLE

Enzymatic activity and thermoresistance of improved microbial transglutaminase variants

B. Böhme[1] · B. Moritz[1] · J. Wendler[1] · T. C. Hertel[1] · C. Ihling[2] · W. Brandt[3] · M. Pietzsch[1]

Received: 28 January 2019 / Accepted: 17 July 2019 / Published online: 26 July 2019

Abstract

Microbial transglutaminase (MTG, EC 2.3.2.13) of *Streptomyces mobaraensis* is widely used in industry for its ability to synthesize isopeptide bonds between the proteinogenic side chains of glutamine and lysine. The activated wild-type enzyme irreversibly denatures at 60 °C with a pseudo-first-order kinetics and a half-life time ($t_{1/2}$) of 2 min. To increase the thermoresistance of MTG for higher temperature applications, we generated 31 variants based on previous results obtained by random mutagenesis, DNA shuffling and saturation mutagenesis. The best variant TG^{16} with a specific combination of five of seven substitutions (S2P, S23Y, S24 N, H289Y, K294L) shows a 19-fold increased half-life at 60 °C ($t_{1/2}$ = 38 min). As measured by differential scanning fluorimetry, the transition point of thermal unfolding was increased by 7.9 °C. Also for the thermoresistant variants, it was shown that inactivation process follows a pseudo-first-order reaction which is accompanied by irreversible aggregation and intramolecular self-crosslinking of the enzyme. Although the mutations are mostly located on the surface of the enzyme, kinetic constants determined with the standard substrate CBZ-Gln-Gly-OH revealed a decrease in K_M from 8.6 mM (±0.1) to 3.5 mM (±0.1) for the recombinant wild-type MTG and TG^{16}, respectively. The improved performance of TG^{16} at higher temperatures is exemplary demonstrated with the crosslinking of the substrate protein *β*-casein at 60 °C. Using molecular dynamics simulations, it was shown that the increased thermoresistance is caused by a higher backbone rigidity as well as increased hydrophobic interactions and newly formed hydrogen bridges.

Keywords Microbial transglutaminase · Thermoresistance · Optimization · Shuffling · Protein crosslinking

Introduction

Microbial transglutaminases (MTG, EC 2.3.2.13) concatenate proteins by catalyzing the formation of an isopeptide bond between the γ-amide of glutamine and the ε-amino group of lysine to form ε-(γ-glutamyl)lysine crosslinks. *S. mobaraensis* TG (wild-type MTG, *Sm*TG) finds its application mainly in the food industry for gelling of casein in milk and restructuring meat (Yokoyama et al. 2004) but is also used in the pharmaceutical, material or textile industry (Zhu and Tramper 2008). However, activity is restricted to mesophilic pH and temperature because at acidic conditions below a pH of four or temperatures above 50 °C *Sm*TG loses rapidly its activity. For example, after treatment at 50 °C for 30 min, 50% of the initial activity is lost (Kieliszek and Misiewicz 2014). Therefore, an MTG with improved thermal resistance would be beneficial to extend the range of applications and increase sustainability of production processes.

Thermodynamic stability is described as a reversible system between the native (N) and unfolded (U) state of

Handling Editor: E. Agostinelli.

Electronic supplementary material The online version of this article (https://doi.org/10.1007/s00726-019-02764-9) contains supplementary material, which is available to authorized users.

✉ M. Pietzsch
markus.pietzsch@pharmazie.uni-halle.de

[1] Department of Downstream Processing, Institute of Pharmacy, Faculty of Sciences I, Martin Luther University Halle-Wittenberg, Weinbergweg 22, Halle (Saale) 06120, Germany

[2] Department of Pharmaceutical Chemistry and Bioanalytics, Institute of Pharmacy, Faculty of Sciences I, Martin Luther University Halle-Wittenberg, Wolfgang-Langenbeck-Str. 4, Halle (Saale) 06120, Germany

[3] Department of Bioorganic Chemistry, Leibniz Institute of Plant Biochemistry, 06120 Halle (Saale), Germany

a protein. The native state is at the global minima of free energy (ΔG) and, therefore, the folding path to the native state is favored under physiologic conditions (Baker and Agard 1994; Sanchez-Ruiz 2010). Kinetic stability not necessarily favors refolding pathway to the native state, but traps the native state by a high unfolding barrier (Sanchez-Ruiz 2010). The high unfolding barrier leads to slow unfolding, which is usually associated with an increase in half-life ($t_{1/2}$) (Brissos et al. 2014; Manning and Colón 2004; Sanchez-Ruiz 2010; Sohl et al. 1998). Often thermodynamic and kinetic stability influence each other. Since steady-state constants as the thermodynamic stability are inaccessible with active MTG due to auto-crosslinking, we use the term "thermoresistance" in the present manuscript and describe the temperature dependence of the kinetic stability.

So far improvement of thermoresistance of recombinant MTG was carried out by random mutagenesis, saturation mutagenesis, DNA shuffling and genetic code expansion as well as for MTG from *Streptomyces hygroscopicus* (*Sh*TG) by saturation mutagenesis and N-terminal deletion.

The first attempt to screen for thermoresistant variants of *Sm*TG was based on the recombinant soluble expression of pro-MTG in *E. coli* BL21 Gold (DE3) (Marx et al. 2007). The established activation and purification process of the recombinant wild-type MTG yields MTG with an N-terminal extension (FRAP) and a C-terminal His_6-tag and was later on termed FRAP-MTG. Marx et al. used random mutagenesis to generate a library with targeted single amino acid substitutions. Out of that library 5500 mutants were screened using a micro titer-plate assay, leading to the identification of six variants with increased thermoresistance. The six variants showed either single or double amino acid substitutions (Marx et al. 2008b). One of these variants, showing the amino acid exchange S2P, exhibits an increased thermoresistance at 60 °C by a factor of 2.7 (recombinant wild-type FRAP-MTG shows a half-life ($t_{1/2}$) of 2 min and FRAP-MTG(S2P) 4.6 min at 60 °C, respectively). Interestingly, the S2P mutation leads also to a higher specific activity at 37 °C using the standard substrate CBZ-Gln-Gly-OH. The six positions with beneficial mutations identified by Marx et al. were then individually screened by saturation mutagenesis for the best amino acid at each position (Buettner et al. 2012). Next, the selected mutant DNAs were used as templates in a shuffling experiment, leading to the identification of eight FRAP-MTG variants with combinations of single mutations which exhibit increased thermoresistance compared to the single mutation variants. The best of these combinatorial variants, called UH308-B, contains three amino acid substitutions at the position 23, 24, and 294 and exhibits an increasing thermoresistance of $t_{1/2} = 24.3$ min (Buettner et al. 2012). Due to the random fragmentation process, Buettner et al. found only eight of the 64 theoretically possible variants, although about 1500 clones were screened.

Recently, genetic code expansion was used to increase the thermoresistance of MTG from *S. mobaraensis* (Ohtake et al. 2018). By incorporation of 3-chlorotyrosine at positions 20, 62 and 171, the half-life at 60 °C could be increased by a factor of 5.1. In an attempt to improve the homologous *Sh*TG (79% sequence identity to mature *Sm*TG) by a combination of N-terminal deletions and saturation mutagenesis, a Del-4 mutant with a 1.8-fold higher specific activity and a 2.7-fold prolonged half-life at 50 °C was discovered ($t_{1/2} = 10.1$ min) (Chen et al. 2012). Unfortunately, experimental data at higher temperatures were not reported.

In the present study, a directed combinatorial approach was used to construct the 31 thermoresistant variants based on the previously determined substitutions (Buettner et al. 2012; Marx et al. 2008b). All variants were characterized with regard to their half-life at 60 °C and specific activity against the standard substrate CBZ-Gln-Gly-OH. Substrate turnover by recombinant FRAP-MTG and thermoresistant FRAP-MTG variants with CBZ-Gln-Gly-OH and *β*-casein as a model protein was assayed at temperatures up to 60 °C, showing the superior activity of a new thermoresistant FRAP-MTG variant at elevated temperatures. Investigations on the mechanism of heat-induced inactivation were carried out by differential scanning fluorimetry (DSF) of active and inactive MTG. The results provide intriguing starting points for further improvements by molecular engineering.

Materials and methods

General

Unless otherwise stated, all chemicals were of analytical grade and were purchased from Carl-Roth GmbH (Karlsruhe, Germany). Enzymes and buffers for restriction-ligation were purchased from Thermo Fisher Scientific (Waltham, U.S.A). Enzymes for cell lysis were lysozyme (egg white) from Sigma-Aldrich (St. Louis, USA) and Benzonase® from Merck Millipore (Billerica, USA). His GraviTrap for small-scale purification was purchased from GE Healthcare (Little Chalfont, United Kingdom). CBZ-Gln-Gly-OH for activity-assay according to (Folk and Cole 1966) was purchased from Bachem AG (Bubendorf, Switzerland). *β*-Casein was purchased from Sigma-Aldrich (purity according to the manufacturer ≥ 98% (PAGE)).

Bacterial strains

Escherichia coli BL21Gold (DE3) was purchased from Novagen (Amsterdam, The Netherlands).

Golden Gate cloning

For combination of the previously identified hot spots S2P, S23Y-Y24 N, G257S, K269S, H289Y and K294L, a method based on the seamless restriction by type II restriction enzyme was used (Engler et al. 2009). Since the S2P mutation leads not only to increased thermoresistance, but also to an increased specific activity by a factor of 1.8, it was decided to keep this mutation in all possible variants. Additionally, because of the close proximity of the mutation S23Y and Y24 N, these positions were kept in only one fragment. As a result, 11 fragments were designed: six fragments each containing the S2P, S23Y-Y24 N, G257S, K269S, H289Y or K294L mutation and 5 fragments harboring the wild-type sequence. Design of the donor and acceptor vector, as well as restriction-ligation reaction were done according to (Engler et al. 2009). In short, each fragment was flanked by the restriction site encoding for the type IIs endonuclease *Bsa*I. The recognition site for *Bsa*I was oriented in a way that the enzyme cleaves outside the recognition site and the fragment is released from the donor vector. As donor vector, the pHSG3988 was used harboring a resistance gene for chloramphenicol. The acceptor vector was pET28a coding for a kanamycin resistance gene in which the LacZ fragment was cloned in the multiple cloning site. The LacZ fragment was flanked by *Bsa*I and is positioned in a way that the LacZ gene is released after treatment with *Bsa*I. Cloning of the donor and acceptor vectors was done by GeneScript Corp. (Hong Kong, China). Restriction and ligation of fragments for each variant were done in a single tube with 100 ng of dephosphorylated donor vector, 50 ng acceptor vector, 10 U of *Bsa*I, 15 U T4-DNA-Ligase and 4 mM ATP in ligase buffer (Thermo Fisher Scientific, Waltham, USA). Reaction conditions were 50 cycles of 5 min restriction at 37 °C and 5 min ligation at 16 °C with a final restriction at 50 °C for 30 min (Engler et al. 2009). Inactivation of enzymes was done for 15 min at 80 °C. All constructs were controlled by restriction analysis using *Xho*I and *Nco*I and sequencing. Sequencing was done by Eurofins Genomic (Ebersberg, Germany). The resulting constructs were named consecutively with subscripted numbers (TG^n, $n = 3–34$, see Table S1 in the supplement for a complete list) and transformed into BL21 Gold (DE3) using chemical transformation method based on (Hanahan 1983).

Expression and cultivation

Production of the variants was carried out using 0.5 L shake flasks using 200 mL minimal medium (Wilms et al. 2001) supplemented with 25 mM Na_2HPO_4, 25 mM K_2HPO_4, 50 mM NH_4SO_4, 5 mM Na_2SO_4, 0.5% glycerol, 0.05% glucose, 0.2% α-lactose,2 mM $MgSO_4$ according to (Studier 2014) and 50 µg/mL kanamycin. Cultivation was carried out at 28 °C and 110 rpm for 20–22 h (Multitron II, Inforce HT, Bottmingen, Switzerland). Cells were harvested by centrifugation for 10 min at 17.700 g and 4 °C and subsequently stored at − 20 °C.

Cell lysis, activation and purification of the variants

Cell lysis was done by enzymatic hydrolysis combined with freeze–thaw cycles. For this, 1.6–1.8 g frozen bio wet mass was suspended in 5 mL lysis buffer (50 mM TRIS/HCl with pH = 8.0, 0.2 mg/mL lysozyme, 1 mM $MgCl_2$, 250 U/mL Benzonase) and incubated for 60 min at 37 °C. Subsequently, three repeated freeze–thaw steps (15 min − 80 °C and 15 min 25 °C) were carried out. Following cell disintegration, samples were centrifuged for 20 min at 17.700 g and 4 °C and the resulting supernatant was treated with 0.6 U/mL proteinase K (Thermo Fisher Scientific, Waltham, U.S.A). Treatment with proteinase K was done for 60 min at 37 °C and is necessary for activation of pro-MTG leaving only an N-terminal FRAP extension (Sommer et al. 2012). After activation, imidazole and NaCl were added to a final concentration of 20 mM and 300 mM, respectively. Purification of FRAP-MTG variants from the supernatant was done using His GraviTrap columns according to the manufacturer's protocol. Binding and equilibration buffer was 50 mM TRIS/HCl (pH = 8.0), 20 mM imidazole, 300 mM NaCl and elution buffer was 50 mM TRIS/HCl (pH = 8.0), 500 mM imidazole, 300 mM NaCl. Fractions were collected and analyzed by the colorimetric hydroxamate procedure (Folk and Cole 1966). Fractions with volumetric activity higher than 30 U/mL were pooled and twice dialyzed against 4 L of 50 mM TRIS/HCl (pH = 8.0) at 4 °C. During dialysis, FRAP-MTG variants precipitate and were harvested at 4 °C and 16.100 g for 2 min after adding DTT with a final concentration of 1 mM in the dialysate. Supernatant was discarded and wet MTG precipitates were aliquoted and stored at – 80 °C.

Inactivation kinetic of the variants and transition temperature (T_M)

Frozen MTG precipitates were solubilized in 0.5 mL 200 mM TRIS/acetate buffer (pH = 6.0) for 30–60 min on ice and centrifuged for 5 min at 16.100 g, and protein concentration was determined using UV absorption at 280 nm. The theoretical extinction coefficient of each variant was calculated using ProtParam (Gasteiger et al. 2005). Protein concentration was adjusted to 0.3 mg/mL. 35 µL of 0.3 mg/mL enzyme solution was transferred into a pcr tube and incubated at the respective temperature. For each time point of a variant, one pcr tube was used. The enzyme solution was incubated for 240 min. For the first 60 min, pcr tubes were processed in 2 min intervals, and for the remaining

time activity was assayed every 30 min. After heat treatment, tubes were subsequently chilled on ice, preventing further inactivation. Each tube was then centrifuged for 3 min at 2000 g and 10 µL of the supernatant was used in the standard hydroxamate assay to detect residual activity (Folk and Cole 1966). For this, 140 µL substrate solution (214.3 mM TRIS/acetate, 107.14 mM hydroxylamine, 10.7 mM reduced glutathione, 32.14 mM CBZ-Gln-Gly-OH) was pre-incubated for 3 min at 37 °C and reaction was started with 10 µL enzyme solution. After 10 min at 37 °C, reaction was stopped by adding 150 µL stop solution (1 vol. 3 M HCl, 1 vol. 12% trichloroacetic acid, 1 vol. 5% $FeCl_3 \times 6H_2O$ (in 0.1 M HCl)). For each time point, the residual activity was determined in duplicate. After reaction was stopped, samples were centrifuged at 16.100 g and 4 °C for 1.5 min and 200 µL of the supernatant was transferred to a clear 96-well plate (MTP Falcon 1172, 96). Absorption at 525 nm was measured using a microtiter plate reader (FluoStar, BMG Labtech GmbH, Offenburg, Germany). Specific activity was calculated by determining the volumetric activity of a 0.05 mg/mL enzyme solution measured with the standard hydroxamate assay. Half-life times were calculated by fitting data points to exponential first-order decay using OriginPro 2016G (OriginLab Corp, Northampton (M), USA).

Transition temperature analysis was done by solubilizing precipitated enzyme in 0.02 M sodium phosphate buffer (pH = 6) for 30–60 min on ice. Enzyme solution was centrifuged for 5 min at 16.100 g and protein concentration was determined using UV absorption at 280 nm. Protein concentration was set to 1 mg/mL and used to fill provided capillaries for the Prometheus NT.48 nanoDSF (NanoTemper Technologies GmbH, Munich, Germany). Heating rate was set to 1 °C/min and identification of onset (T_{on} and T_{agg}) for unfolding and aggregation as well as transition temperature (Tm) was done by NT PR.ThermControl software.

Molecular dynamics simulations

To rationalize and understand the increased thermoresistance caused by the mutations, molecular dynamics simulations (MDS) were carried out using the program YASARA (Krieger et al. 2009) and the embedded AMBER03 force field using the crystal structure of the microbial transglutaminase from *Streptomyces mobaraensis* (Protein Data Bank code: 1IU4, Kashiwagi et al. 2002). Corresponding to TG[16], the following mutations were introduced: S2P, S23Y, Y24 N, H289Y, K294L and the resulting new protein were energy optimized. Subsequently, MDS were carried out for 50 ns at 298 K and for 100 ns at 333 K for both the *Sm*TG and TG[16]. Periodic boundary conditions with a box filled with explicit water molecules and neutralized by NaCl counter ions were applied.

Determination of specific activity

Frozen MTG precipitates were solubilized in 0.5 mL 200 mM TRIS/Acetate (pH = 6.0) for 30–60 min on ice and centrifuged for 5 min at 16.100 g, and protein concentration was determined using UV absorption at 280 nm as described above. Protein concentration was set on 0.05 mg/mL. Volumetric activity was determined with the standard hydroxamate assay (Folk and Cole 1966). For this, 455 µL substrate solutions were pre-incubated for 3 min at 37 °C in thermomixer. After pre-incubation, reaction was started with 70 µL enzyme solution and stopped after 10 min with stop solution. Samples were centrifuged and absorption at 525 nm of the supernatant was measured as described above. One unit of MTG activity is defined as the production of 1 µmol L-glutamic acid γ-monohydroxamate per min at 37 °C.

Determination of kinetic parameters

The kinetics of the conversion of the standard substrate CBZ-Gln-Gly-OH by the FRAP-MTG variants were analyzed with the continuous glutamate dehydrogenase (GDH) coupled assay (Day and Keillor 1999; Oteng-Pabi and Keillor 2013). All measurements were performed at 37 °C in UV cuvettes, using the Ultrospec 2100 pro photometer (Amersham Biosciences).

The reaction buffer contained final concentrations of 200 mM MOPS/KOH (pH 7.2), 1 mM EDTA, 10 mM α-ketoglutarate, 0.5 mM NADH, 0-30 mM CBZ-Gln-Gly-OH, 10 mM glycine methyl ester, 25 U/mL GDH in a final volume of 950 µL. The buffer was pre-incubated for 7 min at 37 °C and the reaction was started by the addition of 50 µL MTG solution (final concentration 0.2 U/mL). The oxidation of the cosubstrate was continuously measured via absorbance measurement at 340 nm. The background oxidation of NADH was subtracted by carrying out a measurement without CBZ-Gln-Gly-OH.

The linear fitting of the slopes of the kinetic curves was carried out with the program OriginPro 2016G (OriginLab Corp, Northampton (M), USA) and the reaction rates were calculated by dividing the slopes by the molar extinction coefficient of NADH (6220 $M^{-1} \times cm^{-1}$). Reaction rates were plotted as a function of substrate concentration to obtain Michaelis–Menten plots. Determination of the kinetic parameters K_M, V_{max} and k_{cat} was done according to Michaelis–Menten equations:

$$v = \frac{V_{max} \times [S]}{K_M + [S]}. \quad (1)$$

where v is the velocity of the reaction, V_{max} is the maximal velocity, [*S*] is the substrate concentration and K_M is the substrate concentration for half-maximal velocity.

Investigation of FRAP-MTG self-crosslinking and turnover of β-casein

For detection of self-crosslinking of TG^{16} and TG^{16} Q328 substitution variants, 50 µL of heat-treated sample was taken at different time points and transferred into 95 °C preheated sample buffer. Polyacrylamide gel electrophoresis (PAGE) was performed according to the method of (Laemmli 1970). Separation was done in 4.5% stacking gel and 12.5% separating gel. Gels were stained overnight with staining solution (1 g/L Coomassie Brilliant Blue G250, 20% isopropanol, 10% acetic acid) and destained in a destain solution (20% isopropanol, 10% acetic acid). Bands were cut out and analyzed by LC/MS.

To investigate crosslinking of a model protein as a macromolecule, 1 mg/mL *β*-casein was dissolved in 200 mM MOPS/KOH buffer (pH = 7.2). Turnover of *β*-casein was assayed at 37 °C and 60 °C catalyzed by 10 U/g (*β*-casein) of the respective FRAP-MTG variant using densitometry. Pictures were captured by G:Box and the GeneSys program and evaluation of band intensity was done with the GeneTools program (Syngene International). Plotting of decreasing band intensity versus time was done with the program OriginPro 2016G.

LC/MS analysis of self-crosslinked FRAP-MTG variants

Gel bands (see above) were processed by *in-gel* digestion with trypsin following standard protocols (Shevchenko et al. 2007). LC/MS analysis of the generated peptide mixtures was carried out on an Ultimate 3000 RSLC nano-HPLC system (precolumn: Acclaim PepMap, 300 µm × 5 mm, 5 µm, 100 A, Thermo Fisher Scientific, separation column: self-packed PicoFrit emitter column, 75 µm × 250 mm, New Objective, packed with 1.9 µm RP-C18 particles, Reprosil-Pur 120, Dr. Maisch) coupled to an Orbitrap Fusion mass spectrometer equipped with a nano-ESI source Nanospray Flex Ion Source (both Thermo Fisher Scientific). After loading and washing the precolumn for 15 min with water containing 0.1% trifluoroacetic acid (flow rate 30 µl/min), peptides were eluted and separated using a gradient from 3 to 30% B over 90 min with a constant flow rate of 300 nL/minute (solvent A: water containing 0.1% formic acid; solvent B: acetonitrile containing 0.08% formic acid). Data were acquired in data-dependent MS/MS mode using stepped HCD (high energy collisional dissociation, normalized collision energies: 26, 29, 32%). Each high-resolution full scan (m/z 300–1500, *R* = 120,000) in the orbitrap was followed by high-resolution product ion scans (*R* = 15,000, min precursor charge state 3^+) within 5 s, starting with the most intense signal in the full scan mass spectrum (isolation window 2 Th); the target value and maximum accumulation time were 50,000 and 200 ms. Dynamic exclusion (duration 60 s, window ± 2 ppm) was enabled. To identify crosslinked products, raw data were converted into Mascot generic format (mgf) files using the Proteome Discoverer 2.0 (Thermo Fisher Scientific). Crosslinked products were identified with the in-house software StavroX 3.6.6. MS and MS/MS data were automatically analyzed, annotated and manually verified.

Results

Generation of mutant library

To identify enzymes with increased thermoresistance, we took advantage of the previously identified single amino acid substitutions by Buettner et al. (S2P, S23Y-Y24 N, G257S, K269S, H289Y and K294L) and generated a library of 32 variants comprising combinations of the individual point mutations (all variants generated are listed in Table S1, supplement). All clones in the library contained the S2P mutation which is known to cause not only increased thermoresistance, but also an increased specific activity. The library was generated by specifically combining six fragments by Golden Gate cloning (Engler et al. 2009), containing either one single mutation or not. The adjacent mutations S23Y and Y24 N were treated as a single mutation and cloned via one fragment leading to five fragments with mutations and a combinatorial library of $2^5 = 32$ variants. The coding sequences of all 32 variants were verified by DNA sequencing. Variants are consecutively numbered and expressed as superscript TG^n ($n = 1$–32, Table S1, supplement). All 32 expression plasmids were transformed into *E. coli* BL21 Gold (DE3) and 31 target proteins were produced and purified (Marx et al. 2008a). Briefly, the C-terminally His_6-tagged pro-enzymes were activated by Proteinase K, leaving an N-terminal FRAP extension, and purified by Ni^{2+}-NTA chromatography. Variant TG^{09} could not be overexpressed nor purified to any significant amount. The purified and active TG^n variants were subjected to the screening procedure.

Screening for thermoresistant variants

To determine the thermoresistance of the purified TG^n variants, the half-life ($t_{1/2}$) was investigated by incubating the variants for different time points at 60 °C. After incubation the residual activity at 37 °C (Folk and Cole 1966) using the artificial substrates CBZ-Gln-Gly-OH and hydroxyl amine was determined. The residual activity of all variants

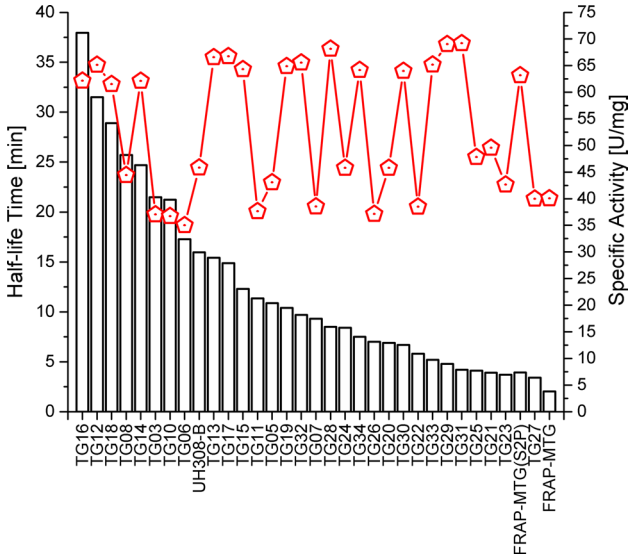

Fig. 1 Half-life times and specific activity of recombinant wild-type FRAP-MTG and all constructed variants: The remaining activity was measured using non-thermal treated sample as 100%. For each time point of a variant, one pcr tube was used. The samples were incubated for 240 min at 60 °C. For the first 60 min, samples were processed every 2 min, for the remaining time activity was assayed every 30 min. Specific activity (A_{spec}, pentagons) was calculated by determining the volumetric activity of a 0.05 mg/mL enzyme solution measured with the standard hydroxamate assay (Folk and Cole 1966). Half-life times were calculated by fitting data points to exponential first-order decay

declined in an exponential first-order fashion and was analyzed by fitting the data to a first-order decay to extract and compare the half-life time of each TG^n variant (Table S1, Fig. 1). All decay curves fit well with the single exponential model with R^2 values of 0.97–0.99, meaning first that the protein irreversibly loses activity at elevated temperatures as described earlier (Ando et al. 1989; Marx et al. 2008b; Menéndez et al. 2006) and second that the process of inactivation can be described with a single macroscopic decay constant enabling a direct correlation of mutation and thermoresistance. Determined half-lives for all variants including the previously identified UH308-B-variant and the FRAP-MTG are listed in Table S1 in a descending order of thermoresistance. An example of a typical inactivation kinetic can be seen in Fig. S1 (Supplement).

At 60 °C, the introduced mutations cause an increase in half-life time from $t_{1/2} = 2$ min (FRAP-MTG) to up to 38 min (TG^{16}) reflecting an up to 19 fold increase in thermoresistance. Although all single mutations have been found to be beneficial, the combinations now show that the impact of each individual mutation is not simply additive. For example, the mutant TG^{03} comprising all mutations is not the one which exhibits the highest thermoresistance. The mutation K269S seems to have a negative effect compared to variants without it. On the other hand, the best 50% of the variants contain the double mutation S23Y-Y24 N showing a high impact of this double mutation for improving the thermoresistance. Also, the mutation H289Y and K294L appear to be beneficial with regard to increased thermoresistance. In contrast, variants with the mutations G257S can be found in the upper places of the ranking, as well as in the middle and lower parts of the ranking, and seem to have no clear influence on the increased thermoresistance. Altogether this is in accordance with Buettner et al. who reported that the single substitutions K294L and S23Y showed the most pronounced effects on thermoresistance (Buettner et al. 2012).

All tested variants exhibit an increased heat resistance at 60 °C compared to FRAP-MTG. For the best two variants, TG^{16} and TG^{12}, as well as for the previously identified FRAP-MTG(S2P) (TG^{04}), UH308-B and the FRAP-MTG, detailed inactivation kinetics were recorded in three individual experiments (labeled with an asterisk in Table S1, supplement). Determined half-lives for FRAP-MTG and FRAP-MTG(S2P) of 2.02 min and 3.92 min, respectively, are in good agreement with results reported by (Marx et al. 2008b). However, half-life of UH308-B was determined to 15.97 min, in contrast to the reported half-life of 24.3 min (Buettner et al. 2012). The difference might be due to differences in the analysis procedure. To the best of our knowledge, the variants TG^{16} and TG^{12} exhibit the longest half-lives with 37.97 min and 31.51 min, respectively, published so far.

Since not only the thermoresistance, but also the activity of the enzyme might have changed upon mutation, the specific activities of all variants were determined (Fig. 1). The specific activities for CBZ-Gln-Gly-OH as a substrate are not correlated to heat resistance but can be classified into two groups: (1) variants showing a wild-type like specific activity (42 ± 7 U/mg) and (2) variants which are in the same range of the FRAP-MTG(S2P) (65 ± 5 U/mg). These results suggest that the increased specific activity is mainly caused by the single substitution S2P which is present in all MTG variants investigated. In contrast, the mutation G257S is present in all variants showing reduced, wild-type like specific activity, indicating that the G257S mutation reverts the positive effect of the S2P mutation. Since the interaction with the dye Coumassie Brilliant Blue could differ for the individual variants, the protein concentration was determined by measuring the UV absorption and using the theoretical absorption coefficient calculated for each variant. Using the absorption based method, the specific activity of, e.g., FRAP-MTG was determined to be 40.05 U/mg. In the literature, the specific activity of MTG from *S. mobaraensis* is reported to be in the range of 23-27 U/mg when the Bradford assay (Marx et al. 2008b; Sommer et al. 2012; Yokoyama et al. 2010) or HPLC (Yokoyama et al. 2010) is used for protein quantification. In both methods, the protein is denatured prior to analysis. If the specific activity was calculated on the basis

of the protein concentration measured by Bradford assay, the activity value (28.5 U/mg) corresponds to the reported value. Since both TG[12] and TG[16] showed similar specific activity of 65 respectively 62 U/mg, half-life was taken as a selection criterion to characterize only TG[16] in more detail.

Molecular dynamic simulations

To explain the increased thermoresistance of TG[16], molecular dynamic simulations (MDS) were performed. The structure and localization of the introduced mutations are shown in Fig. S2. There are almost no alterations of the overall tertiary structure between the X-ray structure and TG[16] after MDS.

The fluctuations of the Cα-atoms shown by residual mean square deviations (RMSD) as a function of time for TG[16] and *Sm*TG are shown in Fig. 2.

Assessing the backbone rigidity by computation of RMSD values, a trend to higher rigidity for the TG[16] can be seen at 298 K (Fig. 2 (a)) and 333 K (Fig. 2b). Although the computed differences of the RMSD values between TG[16] and *Sm*TG fluctuate over the whole timeline, the results reflect a higher rigidity of the backbone. Therefore, the increased thermoresistance of TG[16] is at least partially a result of increased backbone rigidity.

A detailed inspection of the influence of all five amino acid substitutions with respect to protein stabilization leads to an explanation of the increased thermal resistance of TG[16] on the molecular level. The mutated amino acids of TG[16] all are located on the surface of the enzyme, underlining the influence of surface stability as already found for proteins (Colón et al. 2017; Strickler et al. 2006; Zhao and Arnold 1999). The substitutions S23Y together with Y24 N lead to the formation of a hydrogen bond between the side chains of both residues and thus stabilize the loop structure in this positon which does not occur in *Sm*TG. Mutation of K294L supports hydrophobic interactions between L294 and V271 and the side chain of Y289 (mutation H289Y) stabilizes the beta sheet (β7) by hydrophobic interactions with V30. Because proline adopts only a few conformational states, the flexible N-terminal region is affected by higher rigidity in the S2P variant. Altogether the simulations nicely explain the experimental findings.

Molecular details of inactivation

Detailed knowledge about the mechanism of MTG inactivation upon thermal treatment can open the way for further improvement. Therefore, intrinsic protein fluorescence and light scattering of FRAP-MTG, FRAP-MTG(S2P) and TG[16] were analyzed during the process of inactivation by nano differential scanning fluorimetry (nanoDSF). The thermal transition of the relative fluorescence (F_{350}/F_{330}) as well as

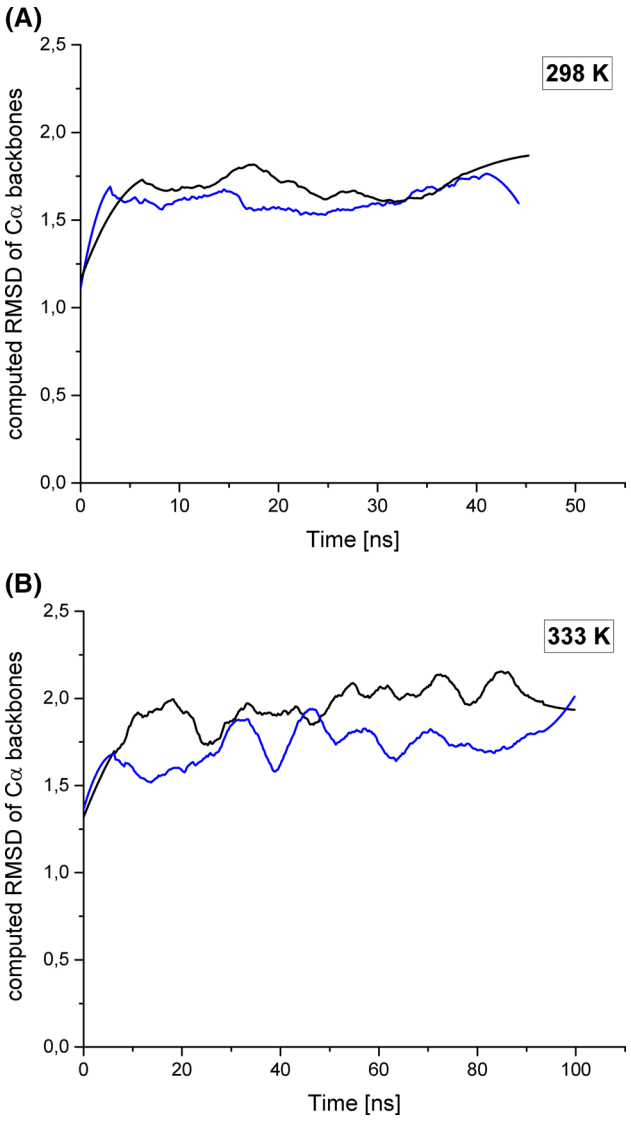

Fig. 2 Computational analysis of backbone rigidity for the TG[16] and FRAP-MTG by Molecular Dynamic Simulation (MDS). Computed RMSD values of TG[16] (blue line) and FRAP-MTG (black line) at 298 K (**a**), respectively, 333 K (**b**). MDS field based on the crystal structure of *Sm*TG (pdb: 1IU4) (Kashiwagi et al. 2002) was done using the program YASARA (Krieger et al. 2009) and the embedded AMBER03 force

the light scatter signal is given in Fig. 3a. The midpoints of the thermal transition of the fluorescence signal, also termed melting points (T_M), can be extracted from the peak of the first derivative of the relative fluorescence signal (Fig. 3b). The determined T_M of FRAP-MTG, FRAP-MTG(S2P) and TG[16] is 58 °C, 59.8 °C and 65.9 °C, respectively. The significant increase in T_M between FRAP-MTG and TG[16] correlates well with the observed prolonged half-life of TG[16] at 60 °C. In addition to the shifted transition curve of FRAP-MTG and TG[16] to higher temperatures the transition of the TG[16] is clearly sharper indicating a pronounced

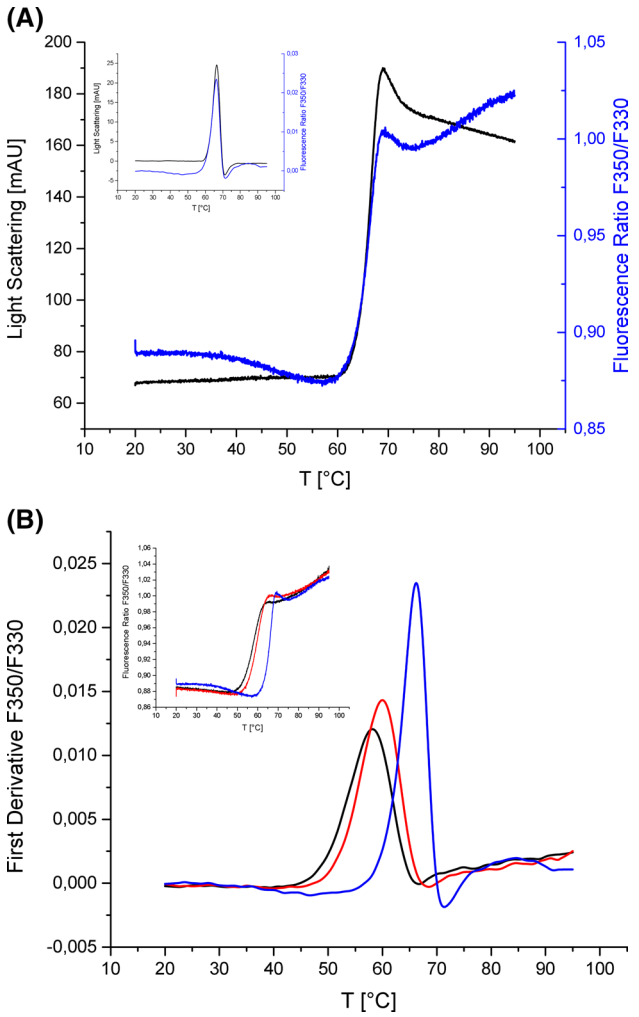

Fig. 3 Temperature scans for unfolding transition of FRAP-MTG, FRAP-MTG(S2P) and TG[16] by determination of the ratio of the fluorescence signal at 350 and 330 nm and light scattering. **a** Comparative representative of aggregation signal (black line) and ratio of fluorescence signal 350/330 (blue line) for the TG[16]. The inset is showing first derivative of 350/330 signal and aggregation signal. **b** First derivative of unfolding curves of FRAP-MTG (black line) and the variants FRAP-MTG(S2P) (red line) and TG[16] (blue line). The inset is showing raw 350/330 signal vs temperature. All measurements were done with differential scanning fluorimetry. Temperature scans were carried out at a protein concentration of 1 mg/mL with a heating rate of 1 °C/min. Scans were recorded in duplicate

cooperativity of the transition process. Surprisingly, the concomitant recorded light scatter signal changes almost congruently to the fluorescence signal upon change in temperature. Hence, the process of unfolding is almost simultaneously followed by the process of aggregation, at least on the macroscopic time scale.

Since (partially) unfolded MTG could be a substrate of (remaining) native MTG we asked whether crosslinking activity directly results in aggregation or the thermal transition process. Therefore, we constructed a catalytically inactive TG[16] where the essential Cys64 is replaced by Serine (TG[16]:C64S) as well as treated a native TG[16] with Iodoacetamide to covalently modify and inactivate the Cys64. Both enzymes had no detectable activity in the standard hydroxamate assay. Analyzing the inactive TG[16] via nanoDSF showed again concomitant aggregation with respect to thermal transition. We conclude that enzyme activity is not a prerequisite of the detected aggregation due to thermal treatment. However, the thermal transition point of inactive TG[16] (C64S or inhibited by Iodoacetamide) measured by nanoDSF increased to 69.5 °C compared to 65.9 °C of the active TG[16] ($\Delta T_M = 3.6$ °C). The remarkable difference of 3.6 °C points toward a direct influence of the crosslinking activity of MTG on its own thermoresistance. The self-crosslinking reaction prevents reversibility of the folding process and accelerates thereby inactivation.

These intriguing findings raised the question whether it is possible to increase thermal resistance further by preventing autocatalytic crosslinking. To follow up this question, we identified the self-crosslinked products which are formed upon thermal treatment. Purified TG[16] was incubated at 65 °C and aliquots were withdrawn at defined time points and analyzed by SDS-PAGE (Fig. 4a). The Coomassie stained gel revealed the time-dependent formation of high molecular weight (hmw) products which are absent at $t = 0$ min, indicating variable numbers of crosslinked TG[16] molecules with intermolecular bonds. Hmw products were also found in comparable experiments for FRAP-MTG and FRAP-MTG(S2P) (data not shown). In addition to the faint hmw bands, a dominant band with higher electrophoretic mobility emerged already at early time points and accumulated over time. To distinguish the two main species, in the following the term xTG is used for the crosslinked TG[16] species showing a higher electrophoretic mobility compared to untreated TG[16]. Although the xTG species does not exhibit any residual activity, it withstands further intermolecular crosslinking and accumulates over time.

If self-crosslinking decreases thermoresistance, the prevention of self-crosslinking might increase heat resistance. To test this hypothesis, we identified crosslinking sites of the xTG product by LC/MS analysis. Several crosslinking sites could be identified (Table S2), but Q328 was almost quantitatively crosslinked to K194, illustrated by less than 1% signal intensity of unmodified Q328 in the treated sample compared to the untreated sample. Obviously, Q328 is a predominant target residue for self-crosslinking. To prevent isopeptide formation at position 328, we generated single-point mutants of the variant TG[16] by replacing Q328 by A, L, V or N and analyzed the crosslinking products by SDS-PAGE (Fig. 4b) and nanoDSF. In opposite to our expectations, the TG[16]-Q328 variants show a decrease in T_M. While the Q328A exchange has only a small effect on T_M from 65.9 °C to 65.1 °C, the Q328 N exchange dramatically decreased the

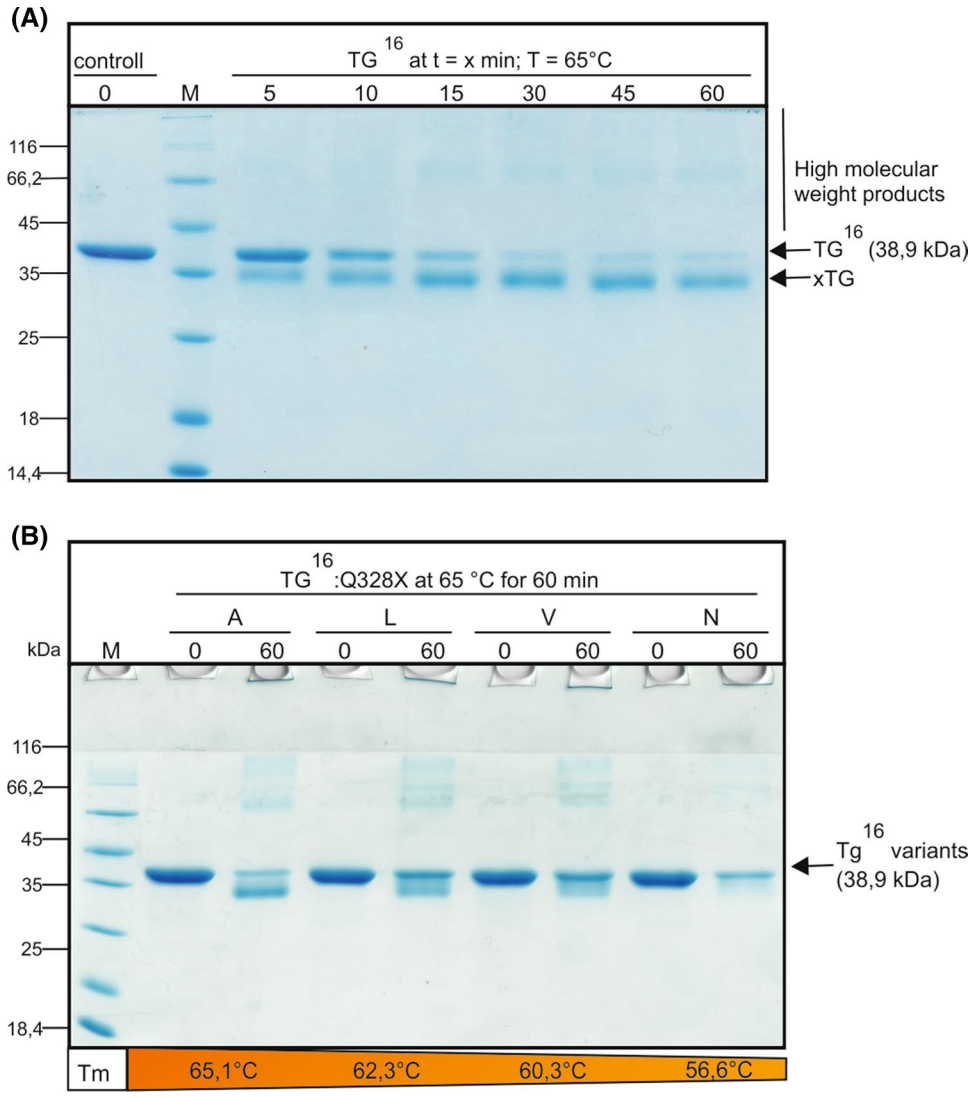

Fig. 4 Self-crosslinking of TG^{16} and TG^{16} variants, in which Q328 was replaced by the amino acids A, L, V and N at 65 °C. **a** Analysis of crosslinked products formed by self-crosslinking of TG^{16} upon incubation at 65 °C over time. **b** Formation of crosslinked TG (xTG) during incubation at 65 °C for 60 min. Enzyme solution of 1 mg/mL was incubated at 65 °C and aliquots were withdrawn at the respective time points and the crosslinking reaction was stopped by direct transfer into 95 °C heated sample buffer

T_M to 56.6 °C. Substitutions of Q328 to V and L had intermediate effects with a T_M of 60.3 °C and 62.3 °C, respectively. The Coomassie stained gel of the auto-crosslinked products reveals a change in the pattern of the crosslinking products of the Q328 variants. As expected, the amount of xTG species is reduced and a slight increase in hmw products as well as in species with an electrophoretic mobility like untreated TG^{16} was observed. Obviously, substituting Q328 indeed reduces the formation of auto-crosslinked products. Although Q328 is substantially involved in auto-crosslinking reactions of the partially unfolded enzyme at elevated temperatures, it contributes substantially to the stability of the protein. As can be seen from the three-dimensional structure, there is a hydrogen bridge between Q328 and the central β7 strand, stabilizing the structure. So the influence of reduced crosslinking of the Q328 exchanges on thermoresistance is superimposed by the essential function of Q328 in stabilizing the MTG. Therefore, a single Q328 exchange should be omitted.

Enzymatic activity

TG^{16} exhibits an increased specific activity compared to FRAP-MTG and FRAP-MTG(S2P). To investigate this in more detail, the kinetic parameters V_{max} and K_M were determined for the substrate CBZ-Gln-Gly-OH. For this purpose, a previously established glutamate dehydrogenase (GDH)-coupled continuous assay was carried out (Oteng-Pabi and Keillor 2013). The activity of FRAP-MTG, FRAP-MTG(S2P) and TG^{16} at different CBZ-Gln-Gly-OH concentrations was measured, while the cosubstrate glycine methyl ester was kept constant at 10 mM. The v-S characteristics were determined and the data points fitted to the Michaelis–Menten equation (Fig. 5). The data points converge

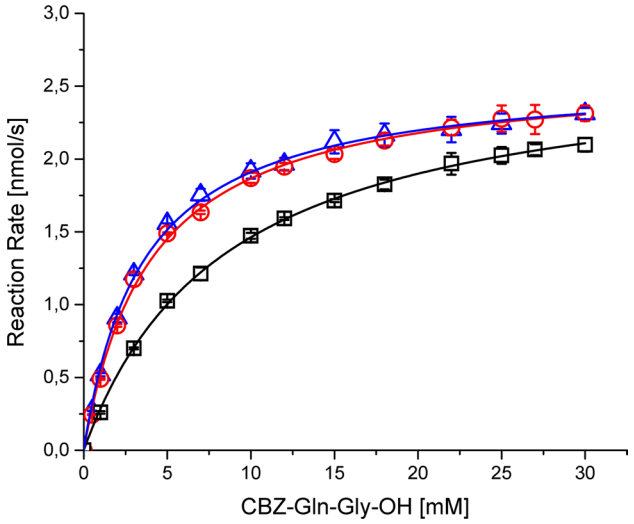

Fig. 5 Determination of the kinetic parameters of FRAP-MTG and the variants FRAP-MTG(S2P) and TG[16]. Release of ammonia was measured using a GDH coupled assay. Reaction was carried out at 37 °C and varying concentrations of CBZ-Gln-Gly-OH (0–30 mM) in the presence of 1 mM EDTA, 10 mM ketoglutarate, 0.5 mM NADH, 10 mM glycine methyl ester and 25 U/mL GDH in 200 mM MOPS buffer. Measurements were done in 1 mL scale using a spectrophotometer. All measurements were done in duplicate. FRAP-MTG (open squares, black), FRAP-MTG(S2P) (open circles, red) and TG[16] (open triangles, blue)

Table 1 Kinetic parameters of recombinant FRAP-MTG (WT), FRAP-MTG(S2P) and TG[16]

	WT	S2P	TG[16]
K_M [mM]	8.55 (±0.96)	4.02 (±0.25)	3.53 (± 0.13)
k_{cat} [s^{-1}]	27.37 (±1.4)	33.92 (±1.13)	32.18 (± 1.13)
k_{cat}/K_M[$s^{-1} \times mM^{-1}$]	3.22 (±0.2)	8.45 (±0.24)	9.10 (± 0.02)
R^2	0.99	0.99	0.99

The kinetic parameters of the three variants were determined as explained in Materials and methods

well ($R^2 = 0.99$) to the simple model and K_M and V_{max} were extracted (Table 1).

Compared to the FRAP-MTG, the FRAP-MTG(S2P) and TG[16] variants are showing approximately a twofold decrease in K_M and a slight increase in k_{cat}. Because we measured specific activity at the technical limit of 30 mM CBZ-Gln-Gly-OH (maximum solubility in the buffer used), the FRAP-MTG variants are not fully saturated with substrate ($K_M = 8.5$ mM). Under those circumstances, a decrease in K_M as measured for S2P and TG[16] impacts the specific activity determination and hence leads to the observed increase in specific activity of S2P and TG[16]. As mentioned earlier, the improved activity toward CBZ-Gln-Gly-OH is predominantly driven by the S2P mutation and explains the small differences in the catalytic parameters between the FRAP-MTG(S2P) and TG[16]. Taken together the improved K_M and k_{cat}-value of TG[16] makes it superior to FRAP-MTG or FRAP-MTG(S2P) at least with regard to the small test substrate. However, besides some applications involving flexible peptide sequences attached to antibodies, e.g., in the field of bioconjugation (Deweid et al. 2018), the major fields of application for MTG are the crosslinking of proteinogenic substrates. To compare the performance of TG[16] with the low molecular weight substrate CBZ-Gln-Gly-OH, the turnover of a proteinogenic substrate (β-casein) was investigated.

Turnover of proteinogenic substrates

The quantification of the reactivity of MTG against a proteinogenic substrate is in principal complicated by the multiplicity of reaction centers. Due to the presence of several glutamine and lysine residues per protein, multiple reactions of a single protein molecule can occur. The complexity of the reaction makes it almost impossible to assign individual rate constants to defined reactions. We, therefore, decided to analyze the decrease of the substrate protein β-casein during the turnover with FRAP-MTG and variants by SDS-PAGE analysis. Due to the crosslinking activity, the band intensity of native β-casein declines and different concatamers appear. The densitometric analysis of the declining β-casein during turnover with FRAP-MTG, FRAP-MTG(S2P) and TG[16] is shown in Fig. 6. The reactions were performed at 37 °C and 60 °C. At 37 °C, the turnover of β-casein by FRAP-MTG and the variants was comparable. The band intensity of native like protein declines continuously in the first 15 min and the decline slows down exponentially in the remaining time. The picture looks different at 60 °C. The turnover by FRAP-MTG proceeds only for the first 5 min and then stops. The turnover by FRAP-MTG(S2P) proceeds roughly for 10 min and is then finished. For the TG[16], the turnover proceeds throughout the tested time of 60 min and β-casein is almost quantitatively converted. The results clearly demonstrate the advantage of the improved half-life of TG[16] compared to FRAP-MTG or FRAP-MTG(S2P). However, the differences in catalytic efficiency between the FRAP-MTG and variants observed with the small test substrate could not be observed with the proteinogenic substrate. The initial rates of β-casein turnover are in the same range. A second advantage of reactions catalyzed by TG[16] is the possibility to work at elevated temperatures that cause (partial) denaturation of substrate proteins which are inaccessible for MTG at ambient temperature. This might open the door for a broader range of substrate proteins than used so far.

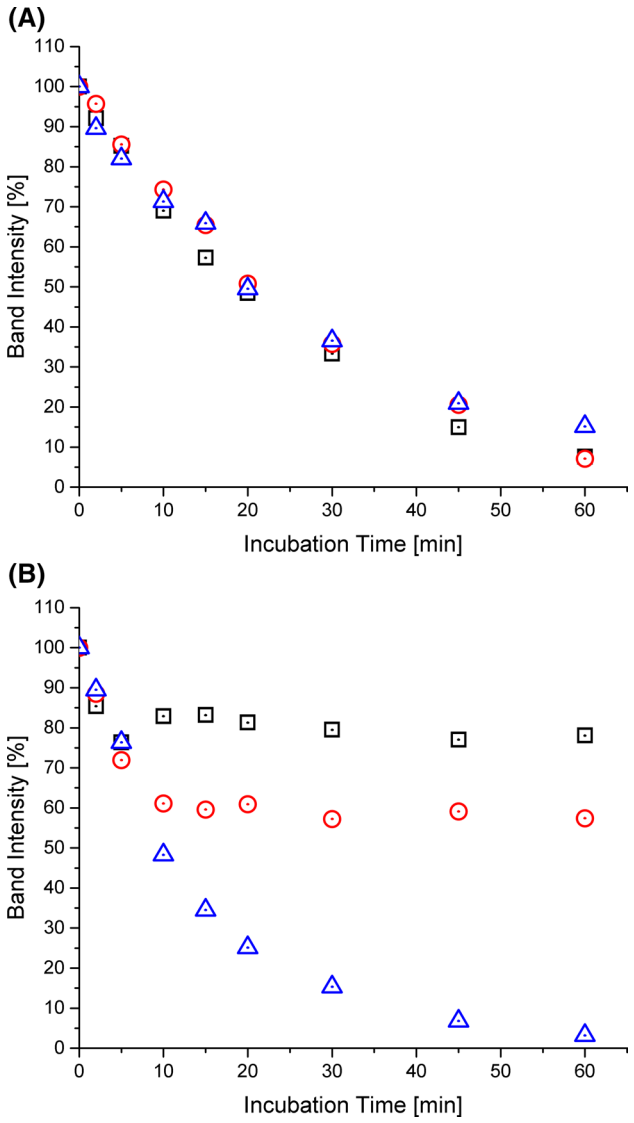

Fig. 6 Cross-linking of β-casein at 37 °C and 60 °C using FRAP-MTG and the variants FRAP-MTG(S2P) and TG[16]. Solutions of 1 mg/mL casein were incubated with 0.0002 mg/mL of either the FRAP-MTG (open squares, black), FRAP-MTG(S2P) (open circles, red) or TG[16] (open triangles, blue) at **a** 37 °C and **b** 60 °C, respectively. Samples were withdrawn at appropriate time periods and immediately transferred to heated SDS sample buffer. Samples were analyzed using SDS-PAGE and a densitometric analysis of the casein monomer band was performed

Discussion

In the present study, thermoresistant recombinant variants of the MTG from *S. mobaraensis* were generated by specific combination of previously determined amino acid substitutions which individually improved thermoresistance (Buettner et al. 2012). Out of 31 tested variants, TG[16] containing the substitutions S2P, S23Y-Y24 N, H289Y and K294L was most resistant at 60 °C, displaying a ~ 19-fold increase in half-life compared to the FRAP-MTG ($t_{1/2}$ = 37.97 min). Comparison of the variants confirmed the important role of the substitutions K294L, S23Y and Y24 N for being most effective in increasing thermoresistance as already suggested (Buettner et al. 2012). Interestingly, combination of individual mutations leads to a synergistic and not simply additive effect. The same findings of combinations of single substitutions were reported for mutations of endo-1,4-xylanase from *Trichoderma reesei* (Turunen et al. 2001) and the xylanase SoxB from *Streptomyces olivaceovirdis* (Turunen et al. 2001; Zhang et al. 2010). MD simulations of MTG revealed that the thermoresistance can be significantly increased by providing stabilization of loop structures (hydrogen bond between S23Y and Y24 N) and hydrophobic interaction to β-sheets (H289Y). The importance of the β-sheet for the thermoresistance of *Sm*TG was already described (Aprodu et al. 2013; Menéndez et al. 2006). Our results show that introduction of hydrogen bonds and increasing hydrophobic interactions led to improved stability of MTG variants which was previously reported also for other enzymes (Shivange and Schwaneberg 2017). Since the observed amino acid exchanges mainly are located on the surface of the TG[16], further studies, e.g., by 3-D-NMR or X-Ray crystallography could be carried out to further investigate the effect of combined substitutions on the enzyme structure.

On a mechanistic point of view, the thermoresistance reported here is strictly correlated with protein stability and arises either from thermodynamic stability, kinetic stability or a combination of both. Usually, thermodynamic stability is measured by differential scanning calorimetry (DSC) or DSF, requiring a reversible equilibrium between native and unfolded state of the protein of interest. As thermal treatment of MTG leads to a fast irreversible aggregation, thermodynamic analysis by DSC/DSF is not possible. Similarly, investigations on the folding and unfolding kinetics are challenging because of fast aggregation of unfolded species, even at low concentrations. Nevertheless, temperature-dependent inactivation kinetics can be interpreted in a way that stabilization of TG[16] is predominantly a result of changes in kinetic stabilization. Experiments to determine the activation energy of inactivation (E_A) yielded E_A values for FRAP-MTG, FRAP-MTG(S2P) and TG[16] of 54, 51.8 and 80.6 kcal/mol, respectively (see Supplement Fig. S3). The drastic increase of E_A for TG[16] indicates that increased thermoresistance is at least in part the result of a kinetic stabilization. On the other hand, kinetic stability is also referred to as long-term stability resulting in an increased half-life ($t_{1/2}$), which is concordant to the increased half-life of TG[16] compared to FRAP-MTG. Additionally, kinetic stability is a common phenomenon for proteins which undergo proteolytic maturation by cleaving a pro-domain of the pro-enzyme (Baker and Agard 1994; Eder and Fersht 1995; Truhlar et al. 2004).

One example is the α-lytic protease, where the pro-domain catalyzes the folding by decreasing the free energy barrier to the native state. Proteolytic cleavage of the pro-region traps the enzyme in a native state. A similar mechanism was already suggested for MTG revealing the importance of the pro-region of MTG for its efficient folding (Rickert et al. 2015; Yurimoto et al. 2004).

Since introducing amino acid substitutions to improve protein stability can lead to detrimental effects on enzymatic activity (Shoichet et al. 1995), specific activity and kinetic parameters of selected variants were determined. Using the small peptide substrate CBZ-Gln-Gly-OH, an improved specific activity and K_M value were observed for TG^{16} compared to the FRAP-MTG. The mutations leading to improved thermoresistance also retained the improved specific activity. The effect of improved kinetic parameters mainly originated from the S2P substitution (Marx et al. 2008b), as shown by comparison of the variants harboring the S2P substitution with variants. This is also confirmed by the kinetic parameters for TG^{16} and the single variant FRAP-MTG(S2P) having a K_M value in the same range and thereby showing that improved catalytic activity is predominantly a result of the S2P substitution. Comparison with previously determined K_M values by Javitt et al. is in good agreement and confirmed our results for the FRAP-MTG as well as for the FRAP-MTG (S2P) (Javitt et al. 2017).

Based on the results of crosslinking reactions with *β*-casein, we were able to show that TG^{16} outperforms the FRAP-MTG and FRAP-MTG(S2P) at 60 °C. For example, after 30 min at 60 °C around 90% of *β*-casein was converted, whereas FRAP-MTG only converted 20% of proteinogenic substrate to product. As a consequence, less amounts of enzyme can be used due to the increased thermoresistance, making a process more cost effective. Concomitant with that, putative substrates having no accessible Gln or Lys at ambient temperatures can be converted to an MTG substrate by unfolding of the structure leading to accessible reactive Gln or Lys and thereby expanding the product range. At 37 °C, however, no differences in the activity between FRAP-MTG and FRAP-MTG(S2P) were found for the crosslinking of *β*-casein. Obviously, the investigation of small peptides does not only insufficiently reflects the properties of natural MTG modification sites (Fiebig et al. 2016) but is also not suited for the prediction of the crosslinking behavior of artificial proteinogenic MTG substrates (as *β*-casein).

The thermal-induced inactivation process of recombinant *Sh*TG (Cui et al. 2008; de Souza et al. 2009; Menéndez et al. 2006) *Bacillus circulans* BL32 *Bc*TG (Cui et al. 2008; de Souza et al. 2009; Menéndez et al. 2006) and *Sm*TG isolated from Activa WM (Menéndez et al. 2006) follow all a pseudo-first-order kinetic. For FRAP-MTG, FRAP-MTG(S2P) and TG^{16} small amounts of unfolded species lead to fast aggregation as determined by nanoDSF. Obviously, the unfolded species cannot populate because they consequently aggregate irreversibly, locking the protein in an inactive state. Although the process of inactivation must be at least a three state process (native, unfolded, inactive) and does not necessarily show inactivation kinetics of pseudo-first order it seems to be a common feature of the MTGs.

To investigate the influence if the self-crosslinking of MTG affects the aggregation behavior, TG^{16} was inactivated by iodoacetamide and by site-directed mutagenesis (TG^{16}:C64S). First, we found that active and inactive variants performed similar in terms of aggregation, showing that aggregation is not driven by self-crosslinking activity. Interestingly, transition temperature of both inactive MTGs shifted by 3.6 °C to higher temperatures. Further investigations showed that self-crosslinking resulted in an accumulating intermediate during heat treatment, called xTG as well as high molecular weight products, showing no residual activity. High molecular weight products are formed by intermolecular crosslinks between MTG molecules. Intramolecular crosslinks resulted in xTG which displayed a higher electrophoretic mobility on the SDS-PAGE compared to untreated TG^{16} and might be a result of a more compact structure.

We could also show that accumulation of xTG is caused by formation of intramolecular isopeptide bonds mainly between Gln 328 and Lys 194. Attempts to prevent self-crosslinking by substitution of Q328 with the amino acids, A, V, L and N, led to different degrees in accumulation of xTG product. For example, the substitution variant TG^{16}:Q328 N showed almost no xTG product, whereas TG^{16}:Q328A showed only minor effects. Determinations of transition temperature showed a very distinctive picture on heat resistance of TG^{16}:Q328 variants, reflecting that (I) position Q328 plays a major role in self-crosslinking and thereby exhibiting a negative effect on thermoresistance and (II) strongly contributing in the stabilization of native structure by beneficial interactions with the other amino acids.

Transglutaminases like MTG (Nieuwenhuizen et al. 2003; Siegmund et al. 2015) and tissue transglutaminases (Schmid et al. 2009) catalyze the formation of inter- and intramolecular crosslinks. To the best of our knowledge, the present contribution is the first report on the formation of intramolecular crosslinks within the MTG.

Knowing the crosslinking sites opens a new approach for rationally engineering the MTG.

Acknowledgements This research was supported by the ''Fachagentur für Nachwachsende Rohstoffe'' (FNR, BMEL, Germany, FKZ 22025814). We are grateful to Prof. Dr. A. Sinz for support in LC/MS analysis. The plasmid for TG^{16}:C64S variant was kindly provided by Nada Zeno Alarake. We also thank M. Anwand for technical assistance.

Compliance with ethical standards

Conflict of interest All authors of this work declare that they have no potential conflict of interest and that there is no financial, consultant, institutional or other relationships that might lead to bias or conflicts of interest in this research. Financial grants, infrastructure and fellowships supporting this work are described in the acknowledgements section.

Human and animal rights statement This article does not contain any studies with human participants or animals performed by any of the authors.

Informed consent Consent to submit this work has been received explicitly from all co-authors. All authors contributed to the scientific work and, therefore, share collective responsibility and accountability for the results.

References

Ando H et al (1989) Purification and characteristics of a novel transglutaminase derived from microorganisms. Agric Biol Chem. https://doi.org/10.1271/bbb1961.53.2613

Aprodu I, Stănciuc N, Banu I, Bahrim G (2013) Probing thermal behaviour of microbial transglutaminase with fluorescence and in silico methods. J Sci Food Agric 93:794–802. https://doi.org/10.1002/jsfa.5799

Baker D, Agard DA (1994) Kinetics versus thermodynamics in protein folding. Biochemistry 33:7505–7509. https://doi.org/10.1021/bi00190a002

Brissos V, Gonçalves N, Melo EP, Martins LO (2014) Improving kinetic or thermodynamic stability of an azoreductase by directed evolution. PLoS One 9:e87209. https://doi.org/10.1371/journal.pone.0087209

Buettner K, Hertel T, Pietzsch M (2012) Increased thermostability of microbial transglutaminase by combination of several hot spots evolved by random and saturation mutagenesis. Amino Acids 42:987–996

Chen K, Liu S, Ma J, Zhang D, Shi Z, Du G, Chen J (2012) Deletion combined with saturation mutagenesis of N-terminal residues in transglutaminase from Streptomyces hygroscopicus results in enhanced activity and thermostability. Process Biochem 47:2329–2334

Colón W, Church J, Sen J, Thibeault J, Trasatti H, Xia K (2017) Biological roles of protein kinetic stability. Biochemistry 56:6179–6186

Cui L, Du G, Zhang D, Chen J (2008) Thermal stability and conformational changes of transglutaminase from a newly isolated *Streptomyces hygroscopicus*. Biores Technol 99:3794–3800

Day N, Keillor JW (1999) A continuous spectrophotometric linked enzyme assay for transglutaminase activity. Anal Biochem 274:141–144. https://doi.org/10.1006/abio.1999.4255

de Souza CFV, Faccin DJL, Mertins O, Heck JX, da Silveira NP, Secchi AR, Ayub MAZ (2009) Kinetics of thermal inactivation of transglutaminase from a newly isolated *Bacillus circulans* BL32. J Chem Technol Biotechnol 84:1567–1575. https://doi.org/10.1002/jctb.2201

Deweid L, Avrutina O, Kolmar H (2018) Microbial transglutaminase for biotechnological and biomedical engineering. Biol Chem. https://doi.org/10.1515/hsz-2018-0335

Eder J, Fersht AR (1995) Pro-sequence-assisted protein folding. Mol Microbiol 16:609–614

Engler C, Gruetzner R, Kandzia R, Marillonnet S (2009) Golden gate shuffling: a one-pot DNA shuffling method based on type IIs restriction enzymes. PLoS One 4:e5553

Fiebig D et al (2016) Structure of the dispase autolysis inducing protein from *Streptomyces mobaraensis* and glutamine cross-linking sites for transglutaminase. J Biol Chem. https://doi.org/10.1074/jbc.m116.731109

Folk JE, Cole PW (1966) Transglutaminase: Mechanistic features of the active site as determined by kinetic and inhibitor studies. Biochimica et Biophysica Acta (BBA)—Enzymology and Biological Oxidation 122:244–264. https://doi.org/10.1016/0926-6593(66)90066-X

Gasteiger E, Hoogland C, Gattiker A, Gattiker SE, Wilkins MR, Appel RD, Bairoch A (2005) protein identification and analysis tools on the ExPASy server. In: Walker JM (ed) The proteomics protocols handbook. Humana Press, NJ, pp 571–607. https://doi.org/10.1385/1-59259-890-0:571

Hanahan D (1983) Studies on transformation of *Escherichia-coli* with plasmids. J Mol Biol 166:557–580. https://doi.org/10.1016/s0022-2836(83)80284-8

Javitt G, Ben-Barak-Zelas Z, Jerabek-Willemsen M, Fishman A (2017) Constitutive expression of active microbial transglutaminase in *Escherichia coli* and comparative characterization to a known variant. BMC Biotechnol 17:23. https://doi.org/10.1186/s12896-017-0339-4

Kashiwagi T, Yokoyama KI, Ishikawa K, Ono K, Ejima D, Matsui H, Suzuki EI (2002) Crystal structure of microbial transglutaminase from *Streptoverticillium mobaraense*. J Biol Chem 277:44252–44260. https://doi.org/10.1074/jbc.M203933200

Kieliszek M, Misiewicz A (2014) Microbial transglutaminase and its application in the food industry. A review. Folia Microbiol. https://doi.org/10.1007/s12223-013-0287-x

Krieger E et al (2009) Improving physical realism, stereochemistry and side-chain accuracy in homology modeling: four approaches that performed well in CASP8. Proteins 77:114–122. https://doi.org/10.1002/prot.22570

Laemmli UK (1970) Cleavage of structural proteins during the assembly of the head of bacteriophage T4. Nature 227:680–685

Manning M, Colón W (2004) Structural basis of protein kinetic stability: resistance to sodium dodecyl sulfate suggests a central role for rigidity and a bias toward β-sheet structure. Biochemistry 43:11248–11254. https://doi.org/10.1021/bi0491898

Marx CK, Hertel TC, Pietzsch M (2007) Soluble expression of a pro-transglutaminase from *Streptomyces mobaraensis* in *Escherichia coli*. Enzym Microb Technol 40:1543–1550. https://doi.org/10.1016/j.enzmictec.2006.10.036

Marx CK, Hertel TC, Pietzsch M (2008a) Purification and activation of a recombinant histidine-tagged pro-transglutaminase after soluble expression in *Escherichia coli* and partial characterization of the active enzyme. Enzym Microb Technol 42:568–575. https://doi.org/10.1016/j.enzmictec.2008.03.003

Marx CK, Hertel TC, Pietzsch M (2008b) Random mutagenesis of a recombinant microbial transglutaminase for the generation of thermostable and heat-sensitive variants. J Biotechnol 136:156–162. https://doi.org/10.1016/j.jbiotec.2008.06.005

Menéndez O, Rawel H, Schwarzenbolz U, Henle T (2006) Structural changes of microbial transglutaminase during thermal and high-pressure treatment. J Agric Food Chem 54:1716–1721. https://doi.org/10.1021/jf0522863

Nieuwenhuizen WF, Dekker HL, de Koning LJ, Gröneveld T, de Koster CG, de Jong GAH (2003) Modification of glutamine and lysine residues in holo and apo α-lactalbumin with microbial transglutaminase. J Agric Food Chem 51:7132–7139. https://doi.org/10.1021/jf0300644

Ohtake K et al (2018) Engineering an automaturing transglutaminase with enhanced thermostability by genetic code expansion with

two codon reassignments. ACS Synth Biol 7:2170–2176. https://doi.org/10.1021/acssynbio.8b00157
Oteng-Pabi SK, Keillor JW (2013) Continuous enzyme-coupled assay for microbial transglutaminase activity. Anal Biochem 441:169–173. https://doi.org/10.1016/j.ab.2013.07.014
Rickert M et al (2015) Production of soluble and active microbial transglutaminase in *Escherichia coli* for site-specific antibody drug conjugation. Protein Sci 25:442–455
Sanchez-Ruiz JM (2010) Protein kinetic stability Biophysical Chemistry 148:1–15. https://doi.org/10.1016/j.bpc.2010.02.004
Schmid AW, Chiappe D, Pignat V, Grimminger V, Hang I, Moniatte M, Lashuel HA (2009) Dissecting the mechanisms of tissue transglutaminase-induced cross-linking of alpha-synuclein: implications for the pathogenesis of Parkinson disease. J Biol Chem 284:13128–13142. https://doi.org/10.1074/jbc.M809067200
Shevchenko A, Tomas H, Havli J, Olsen JV, Mann M (2007) In-gel digestion for mass spectrometric characterization of proteins and proteomes. Nat Protoc 1:2856. https://doi.org/10.1038/nprot.2006.468
Shivange AV, Schwaneberg U (2017) Recent advances in directed phytase evolution and rational phytase engineering. In: Alcalde M (ed) Directed enzyme evolution: advances and applications. Springer International Publishing, Cham, pp 145–172. https://doi.org/10.1007/978-3-319-50413-1_6
Shoichet BK, Baase WA, Kuroki R, Matthews BW (1995) A relationship between protein stability and protein function. Proc Natl Acad Sci USA 92:452–456
Siegmund V et al (2015) Locked by design: a conformationally constrained transglutaminase tag enables efficient site-specific conjugation. Angew Chem Int Ed 54:13420–13424. https://doi.org/10.1002/anie.201504851
Sohl JL, Jaswal SS, Agard DA (1998) Unfolded conformations of [alpha]-lytic protease are more stable than its native state. Nature 395:817–819
Sommer C, Hertel TC, Schmelzer CEH, Pietzsch M (2012) Investigations on the activation of recombinant microbial pro-transglutaminase: in contrast to proteinase K, dispase removes the histidine-tag. Amino Acids 42:997–1006. https://doi.org/10.1007/s00726-011-1016-x
Strickler SS et al (2006) Protein stability and surface electrostatics: a charged relationship. Biochemistry 45:2761–2766. https://doi.org/10.1021/bi0600143
Studier FW (2014) Stable expression clones and auto-induction for protein production in *E. coli*. In: Chen YW (ed) Structural genomics: general applications. Humana Press, NJ, pp 17–32. https://doi.org/10.1007/978-1-62703-691-7_2
Truhlar SME, Cunningham EL, Agard DA (2004) The folding landscape of Streptomyces griseus protease B reveals the energetic costs and benefits associated with evolving kinetic stability. Protein Sci 13:381–390. https://doi.org/10.1110/ps.03336804
Turunen O, Etuaho K, Fenel F, Vehmaanperä J, Wu X, Rouvinen J, Leisola M (2001) A combination of weakly stabilizing mutations with a disulfide bridge in the α-helix region of Trichoderma reesei endo-1,4-β-xylanase II increases the thermal stability through synergism. J Biotechnol 88:37–46. https://doi.org/10.1016/S0168-1656(01)00253-X
Wilms B, Hauck A, Reuss M, Syldatk C, Mattes R, Siemann M, Altenbuchner J (2001) High-cell-density fermentation for production of L-*N*-carbamoylase using an expression system based on the Escherichia coli rhaBAD promoter. Biotechnol Bioeng 73:95–103
Yokoyama K, Nio N, Kikuchi Y (2004) Properties and applications of microbial transglutaminase. Appl Microbiol Biotechnol 64:447–454. https://doi.org/10.1007/s00253-003-1539-5
Yokoyama K, Utsumi H, Nakamura T, Ogaya D, Shimba N, Suzuki E, Taguchi S (2010) Screening for improved activity of a transglutaminase from Streptomyces mobaraensis created by a novel rational mutagenesis and random mutagenesis. Appl Microbiol Biotechnol 87:2087–2096. https://doi.org/10.1007/s00253-010-2656-6
Yurimoto H, Yamane M, Kikuchi Y, Matsui H, Kato N, Sakai Y (2004) The pro-peptide of Streptomyces mobaraensis transglutaminase functions in cis and in trans to mediate efficient secretion of active enzyme from methylotropic yeasts. Biosci Biotechnol Biochem. https://doi.org/10.1271/bbb.68.2058
Zhang S, Zhang K, Chen X, Chu X, Sun F, Dong Z (2010) Five mutations in N-terminus confer thermostability on mesophilic xylanase. Biochem Biophys Res Commun 395:200–206. https://doi.org/10.1016/j.bbrc.2010.03.159
Zhao HM, Arnold F (1999) Directed evolution converts subtilisin E into a functional equivalent of thermitase. Protein Eng. https://doi.org/10.1093/protein/12.1.47
Zhu Y, Tramper J (2008) Novel applications for microbial transglutaminase beyond food processing. Trends Biotechnol 26:559–565. https://doi.org/10.1016/j.tibtech.2008.06.006